Interactions of 100 MeV/nucleon ^{40}Ar with uranium

K. A. Frankel and J. D. Stevenson

Lawrence Berkeley Laboratory, and Department of Physics, University of California, Berkeley, California 94720

(Received 1 February 1980; revised manuscript received 1 December 1980)

Fragments produced in the interactions of 100 MeV/nucleon ^{40}Ar projectiles with a uranium target have been measured at energies from 10 to 130 MeV/nucleon at angles from 10° to 170°. Nuclei with charge $5 \leq Z \leq 10$ were observed. The data can roughly be divided into two groups, corresponding to central and peripheral collisions. The central collision data can be fitted with a thermal model that uses two recoiling sources. The source velocities are consistent with the predictions of the fireball and target explosion models, but the source temperatures inferred from the data are higher than one would expect on the basis of energy and momentum conservation. These results are similar to those obtained in previous studies at beam energies of 400 and 500 MeV/nucleon. The data also follow the pattern of the universal curve of invariant cross section vs momentum observed at higher beam energies by Price *et al*. The projectile fragmentation data are also fitted by two thermal sources. There are indications that the observed temperatures are higher than one would expect on the basis of other projectile fragmentation studies. From this broad survey we conclude that although much of the spectrum can be described by falling exponentials in energy in the emitting frames, the observed spectrum is due to nonequilibrium sources since the temperatures derived from the slopes of the exponentials are greater than those we predict.

[NUCLEAR REACTIONS U(^{40}Ar, B), U(^{40}Ar, C), U(^{40}Ar, N), U(^{40}Ar, O), U(^{40}Ar, F), U(^{40}Ar, Ne), $E = 100$ MeV/nucleon; measured $d^2\sigma/d\Omega dE(E;\theta)$.]

I. INTRODUCTION

Many experiments have been conducted recently to study fragments emitted in relativistic heavy ion collisions.[1] These studies have typically been conducted with projectiles up to mass 56 and energies in the range 250 to 2100 MeV/nucleon. The most copiously produced charged fragments emitted in these collisions are protons, but fragments with mass and charge greater than unity are often seen.

By measuring the distribution of fragments emitted in high-energy nucleus-nucleus collisions we hope to learn about the properties of nuclear matter at greater than normal density and temperature. Heavy ion collisions may provide evidence for nuclear shock waves, density isomers, and Lee-Wick matter.[2] Numerous models have been developed which attempt to explain the distributions of the emitted fragments. Single-particle inclusive cross sections of emitted protons have been qualitatively explained by a number of models, such as nucleus-nucleus cascade,[3-5] firestreak,[6] and nuclear hydrodynamics.[7] These models do not require the existence of exotic phenomena, such as shock waves, to explain the data. Because inclusive measurements average over impact parameter, do not take multiplicity effects into account and may result from a number of processes, the effects of compression or new phenomena may be obscured. Experiments to measure pion and cluster emission ($A_{\text{fragment}} > 1$) and to measure spectra of emitted fragments as a function of multiplicity have been conducted in the hope that some signature of compression or other new phenomena might be seen. In this paper we will primarily be concerned with the study of emission of fragments of medium mass, especially $8 \lesssim A_{\text{fragment}} \lesssim 20$.

High-energy heavy ion collisions have generally been divided into two categories: peripheral collisions, where the colliding nuclei barely graze each other, and central collisions, where there is a large overlap of the colliding nuclei. The peripheral collisions have been understood either as a fast process, where each nucleus splits into two pieces "immediately" after colliding, or as a slow process, where the nuclei fragment only after thermal equilibrium has been attained.[8] Central collisions can be quite violent; many fragments of various sizes can be emitted in a single collision. The mechanism for cluster emission is not well understood. For $2 < A_{\text{fragment}} \lesssim 6$, the thermodynamic[9] and coalescence models[10] have had some success in explaining the distributions, but they do not work well for heavier fragments.[11] The heavier fragments appear to be emitted from a moving thermal source with a velocity and temperature that is inconsistent with energy and momentum conservation. The data for these fragments exhibit an abnormally high temperature. The origin of the phenomenon is not understood but it is suspected that the fragments are emitted prior to the attainment of thermal equilibrium, where the requirement $E = \frac{3}{2} T$ ($k = 1$) need not be satisfied. Another possibility involves the conversion of random motion to radial motion during decom-

pression.[12] The data from a number of experiments appear to lie on a single universal curve when the invariant cross section in the moving frame of the emitting source is plotted as a function of total momentum.[13] The origin of this curve is unknown. Some underlying physics may explain it or it may be an accident.

We hope that further experimentation may lead to an understanding of how fragments are produced in heavy ion collisions. In this paper we present results from the experiment 100 MeV/nucleon $^{40}Ar + U \rightarrow$ fragments ($5 \leq Z_{\text{fragments}} \leq 10$). Angle and energy distributions are measured at angles from 10 to 170 deg and from energies of approximately 10 to 130 MeV/nucleon. By working with a 100 MeV/nucleon beam we can measure fragments through a large rapidity region. Fragments can be observed from both central and peripheral collisions in a single experiment. As 100 MeV/nucleon is a basically unexplored region, we can conduct a survey over a large dynamic range to look for unexpected phenomena and to test the models used at higher energies.

From the measurements to be described below, we find that the cross sections fall steeply with increasing fragment energy at most energies and angles. At 10° there is a projectile fragmentation peak at the beam velocity. At small angles and at rapidities between the target and the beam, the cross sections are either flat or fall slowly.

The data, apart from some points in the forward direction, appear to be due to central collisions and are fitted reasonably well by a model based on the assumption of thermodynamic equilibrium of two sources. One source has a velocity corresponding to the recoil velocity of a system formed when the projectile and target unite to form a single entity. The second source is the "fireball" source which is formed from the overlap of the nuclear matter of the projectile and target. The overlapping nuclei recoil as a single unit while the nonoverlapping piece of the projectile proceeds near the beam velocity and the corresponding target piece remains near zero velocity. The observed temperatures are much higher than energy and momentum conservation would predict. This situation is similar to that observed at higher energies. The data are shown to be consistent with the universal curve of invariant cross section vs momentum, discovered by Price *et al.*[13] The data at very forward angles, which we associate with projectile fragmentation, are fitted by two thermal sources. One source moves at approximately the beam velocity and has a higher temperature than is normally seen in projectile fragmentation studies. The second source has a velocity of $\beta = v/c \sim -0.1$ in the projectile frame. This source may only be an artifact of the parametrization as it overestimates the data at larger angles.

II. SUMMARY OF PREVIOUS DATA AND MODELS

There are a number of experiments and interpretive models that have guided the development of the field of high-energy heavy ion collisions. Here we discuss primarily those experiments and models that have relevance to the subject of this paper.

It is often convenient to divide heavy ion collisions into classes based on impact parameter. At large impact parameter only a small portion of each nucleus is involved in a collision. This is generally referred to as projectile fragmentation or target fragmentation, depending on whether we are looking at particles emitted from the projectile or the target. In these interactions there is little energy and momentum transfer between the target and projectile. At small impact parameters many nucleons are involved in a collision. There is often a large amount of energy and momentum transfer. We should remember that since the impact parameter is a continuous variable, there cannot be a definite separation between interaction regions. When analyzing data we often find that geometrical factors play a major role in our ability to divide collisions into various classes.

A. Central collisions

Let us first consider collisions with small impact parameter. There is a high multiplicity of fragments. They are often produced at large angles and at veloicites between zero and the beam velocity. There is a good deal of overlap of the nuclei. When the projectile is smaller than the target it may be totally enveloped by the target. These interactions are commonly referred to as central collisions.

We can study central collisions by observing proton spectra, fragment spectra of composites ($A > 1$), or pion spectra. Let us assume the energy is low enough so that pion production is negligible. When building a model for the proton spectrum, it is convenient to fit the model to what we call the primordial spectrum. This is the spectrum that would be observed if composite nuclei were not formed. We define the primordial spectrum by the expression

$$\left(\frac{d^2\sigma}{d\Omega dE}\right)_{\text{primordial}} = \sum_{\text{all isotopes}} Z \frac{d^2\sigma(Z,A)}{d\Omega dE}, \qquad (1)$$

where E is the energy/nucleon.

1. Single nucleon emission

The Monte Carlo method can be used to fit the primordial proton spectrum. Stevenson has obtained good fits for the reactions 250 and 400 MeV/nucleon ^{20}Ne + U, 400 MeV/nucleon ^{4}He + U, and 800 MeV/nucleon ^{20}Ne + NaF.[3] In this calculation a relativistic nucleus-nucleus collision is treated as a succession of two-body nucleon-nucleon collisions.

The nuclear fireball[14] and firestreak[6] models have also been used to try to explain the proton data. These models involve the geometry of the collision and equilibrium thermodynamics. The fireball model divides the nucleons into participants and spectators. The colliding nuclei are assumed to make clean cuts through each other. The participants, which contribute to the intermediate energy protons, are the nucleons from the overlapping cylindrical cuts. Conservation of energy and momentum give the velocity and temperature of the resulting fireball.[15] The fireball velocity is given by

$$\beta = \frac{P_{\text{lab}}}{E_{\text{lab}}} = \frac{N_p[t(t+2m_{\text{NB}})]^{1/2}}{(N_p+N_t)m_{\text{NB}}+N_p t}, \tag{2}$$

where P_{lab} is the fireball momentum in the laboratory frame, E_{lab} is the total energy in the laboratory, t is the projectile incident kinetic energy per nucleon in the laboratory, m_{NB} is the mass of a bound nucleon (931 MeV), N_p is the number of projectile participants, and N_t is the number of target participants.

The center of mass (relativistic) energy is given by

$$E = (E_{\text{lab}}{}^2 - P_{\text{lab}}{}^2)^{1/2} = [(N_p+N_t)^2 m_{\text{NB}}{}^2 + 2m_{\text{NB}} N_p N_t t]^{1/2}. \tag{3}$$

The temperature T is given nonrelativistically by

$$T = \frac{2}{3}\left(\frac{E}{N_t+N_p} - m_N\right), \tag{4}$$

where m_N is the mass of a free nucleon (939 MeV). The free nucleon mass m_N is used in Eq. (4) because the fireball is assumed to consist primarily of free nucleons. If light nuclei constitute a significant fraction of the fireball then the fireball temperature will be higher than the value given by Eq. (4). The presence of light nuclei in the fireball raises its temperature because less energy goes into breaking nuclear bonds and there are fewer particles to share the fireball energy.

The fireball, according to this model, then decays with a Maxwellian distribution. Upon integrating over impact parameters one obtains the calculated cross section for protons. The spectators reside in the material of the projectile and target that is not in the overlap region. They decay in their own frames, emitting low-energy fragments.

If the projectile does not make clean cuts, there may be some critical impact parameter for which the fireball does not escape the target nucleus. This is called "target explosion." One can again use energy and momentum conservation to calculate the expected cross sections. It has been pointed out that this mechanism could be responsible for the 10 to 90 MeV protons produced in 400 MeV/nucleon ^{20}Ne on U collisions.[14]

2. Composite fragments

The study of cluster emission has proved to be an interesting problem. Two models that have been used to describe the emission of light fragments are the coalescence model of Gutbrod *et al.*[10] and Mekjian's statistical thermodynamic model.[9]

For fragments of charge greater than two it is convenient to fit the data to models with three or more parameters. If we are using a thermodynamic model we may choose

$$\frac{d^2\sigma}{d\Omega dE} = K\sqrt{E}\, e^{-E/\tau} \tag{5}$$

to be the nonrelativstic cross section in the frame of a moving source. The parameters are K, β, and τ. K gives the overall normalization. τ is often taken to be equal to, or a simple function of the source temperature, and β is the velocity of the source. From the fitted β and τ we can attempt to explain the physics of the reaction. For example, if a fragment were emitted from an infinitely massive source in thermal equilibrium, τ would be the temperature of the source. We should note that the parameters do not refer to a single discrete source, but to an average over a continuum of sources.

Let us consider the reaction 400 MeV/nucleon ^{20}Ne + U → B + anything. For 10 MeV/nucleon $\lesssim E_{\text{fragment}} \lesssim$ 40 MeV/nucleon Gosset *et al.*[15] parametrize their data by $\beta = 0.06$ and $\tau = 27$ MeV. Using Eqs. (2)–(4) we obtain a center of mass velocity of the projectile-target system of $\beta = 0.08$ and a target explosion temperature for a gas of nucleons of 13.5 MeV. The authors claim that the source velocity could mean that these fragments are preferentially emitted by the most central collisions. The system formed then decays by a thermal equilibrium mechanism. The authors say the higher temperature is in the correct direction when composite particles are taken into account in the fireball. For the same reaction in a different experiment Stevenson *et al.*[11] found for 30

MeV/nucleon $\lesssim E_{\text{fragment}} \lesssim 50$ MeV/nucleon that the recoiling source could be fitted with a velocity β of 0.091 and $\tau = 62$ MeV. They claim this is evidence for the production of slowly moving, highly excited nuclear matter. The β and high τ are inconsistent with energy and momentum conservation if τ is taken to be the source temperature. This suggests that the slow source is nonthermal since then the internal energy need not be $\frac{3}{2}\tau$ per nucleon. Ta Cheung[16] has analyzed several reactions and he claims to be able to account for the low velocity (but not the high τ) of the slow source based on the kinematics of the collisions. Recently Randrup and Koonin have developed a statistical model[17] for multifragment final states in nuclear collisions. Their preliminary results qualitatively explain the anomalous high temperatures observed in collisions with bombarding energies $E/A \approx 100$ MeV/nucleon. Further work is in progress.[18]

We can also parametrize the slow source by an exponential in momentum. Price *et al.*[13] have analyzed a number of experiments and have shown that the invariant cross sections of all fragments appear to define a universal curve that is exponential in momentum. They evaluate the momentum in a frame in which the distribution is isotropic. The reason for the existence of the curve is unknown. The authors suggest further experimentation over a wide range of fragment mass and momentum as a test of the applicability of the curve.

B. Peripheral collisions

Let us next consider projectile fragmentation. Greiner *et al.*[19] have observed projectile frame fragments with the 0-deg spectrometer at the Bevalac. They measure fragment momentum distributions that are Gaussian in shape, with small momentum transfer to the projectile nucleus. The fragments are typically measured to a total momentum of 400 MeV/c in the projectile frame. The widths of the Gaussian can be given by

$$\sigma^2 = \sigma_0^2 \frac{K(A-K)}{A-1}, \tag{6}$$

where K is the fragment mass, A is the projectile mass, and σ_0 is a constant, approximately 90 MeV/c.[8]

Goldhaber[8] has shown that projectile fragmentation is consistent with the sudden liberation of virtual clusters or with the attainment of thermal equilibrium. In the sudden model Goldhaber calculates the mean square momentum $\langle p_k^2 \rangle$ of k nucleons chosen at random from a box of A nucleons with mean square momentum $\langle p^2 \rangle$. Using conservation of momentum, it is a simple exercise in combinatorics to show

$$\langle p_k^2 \rangle = \frac{K(A-K)\langle p^2 \rangle}{A-1} \tag{7}$$

with $\langle p^2 \rangle = \frac{3}{5}$ of the square of the Fermi momentum. One can extend this calculation by computing higher moments. These moments could be checked with the higher moments of the Gaussian distribution. This could tell us if we expect fragments with momenta much greater than the Fermi momentum still to be characterized by a Gaussian distribution.

Goldhaber showed that if the projectile nucleus comes to thermal equilibrium and divides into two fragments, then σ is related to the temperature by

$$\sigma^2 = m_N T \frac{K(A-K)}{A}, \tag{8}$$

where the temperature T corresponds to about 9 MeV and m_N is the nucleon mass.

In general there is a parallel width $\sigma_\parallel = \sigma_z$ and a perpendicular width $\sigma_\perp^2 = 2\sigma_x^2 = 2\sigma_y^2$. In high energy reactions it has been found that $\sigma_z \approx \sigma_x \approx \sigma_y \equiv \sigma$.[19] At beam energies of ≈ 100 MeV/nucleon Van Bibber *et al.* have found a contribution to $\sigma_\perp$ due to orbital deflection of the projectile by the nuclear and Coulomb potentials of the target.[20] The transverse width $\sigma_\perp$ is changed to

$$\sigma_x^2 = \sigma_y^2 = \frac{\sigma_\perp^2}{2} = \frac{K(A-K)}{A-1}\sigma_0^2 + \frac{K(K-1)}{A(A-1)}\sigma_1^2, \tag{9}$$

where σ_1^2 is the variance of transverse momentum of the projectile at the time of fragmentation. For oxygen fragmentation on aluminum and gold targets, σ_1 is $\simeq 200$ MeV/c.

Westfall *et al.*[21] have observed the target frame analog of projectile fragmentation. They measured energy spectra of fragments produced with 2.1 and 4.9 GeV proton beams. They used both light (C and Al) and heavy (Ag and U) targets. They fitted their data to a Maxwell-Boltzmann distribution that incorporated two-body breakup kinematics and a Coulomb barrier with smearing. The distribution in the moving frame is

$$\frac{d^2\sigma}{dE^* d\Omega^*} = \frac{\sigma_i}{2(\pi\tau_i)^{3/2}} \sqrt{E^*}\, e^{-E^*/\tau_i}, \tag{10}$$

where E^* is the kinetic energy available in the two-body breakup, σ_i is the total cross section for ith fragment, and τ_i is the temperature. They find the data can be fitted by the sum of two distributions. For light targets the emitting system can be characterized by $\beta_1 = 0.005$, $\tau_1 \sim 7$ MeV, $\beta_2 \sim 0.01$, and $\tau_2 \sim 13$ MeV. For the heavy targets they find $\beta_2 \sim 0.006$ and $\tau_2 \sim 15$ MeV. They interpret the low temperature component to be the result of the sudden breakup of a nucleus involved in a

peripheral collision. The high temperature component is interpreted as being the result of a central collision where there has been a high deposition of energy in the emitting nucleus. The transition to the high energy component occurs at approximately an energy of 10 MeV (or a total momentum ~360 MeV/c) at 90° for ^{7}Be emitted from p + C reactions. It is not too difficult to see the high energy component if we can observe fragments with several hundreds of MeV of kinetic energy.

C. Motivation for the present experiment

We see that measurements have been made over a large kinematic region. The relationships between these results and their correspondence to theory are often difficult to determine. We would like to know as much as possible about a single relativistic heavy ion collision. It would be useful to look at heavy fragments through the entire kinematic range, from near zero velocity to beam velocity and beyond. Such a broad-range experiment has been conducted for proton emission and has given insight into the applicability of various models such as the firestreak model.[22] A broad-range experiment to measure heavy fragments could test various models of composite formation and show where the regions of their applicability exist.

III. DESCRIPTION OF EXPERIMENT

We measured energy and angular distributions of fragments emitted in the collision of 100 MeV/nucleon ^{40}Ar + U. The exposure was made at the Berkeley Bevalac's Irradiation Facility. We used Lexan plastic detectors to measure fragment distributions for $5 \leq Z \leq 10$.

The detector stacks contained between 10 and 400 sheets of 75 μm thick plastic. From previous experience we found that a 10% difference in sheet thickness could cause a 100% change in detection efficiency, especially for particles with low detection efficiency ($\lesssim$20%). We decided to reduce the seriousness of this problem by preselecting our sheets. We measured the thicknesses at four points on each sheet. We rejected sheets if the average thickness or the thickness gradient exceeded a certain limit. Approximately one-third of the sheets were rejected. The stacks were milled to 7.6 × 7.6 cm so that each stack would be of the same area to facilitate aligning tracks in adjacent sheets.

The stacks were mounted in a frame that fitted inside an 2.6 m vacuum chamber. The chamber was 0.6 m in diameter and the stacks were placed at radial distances as far from the beam line as possible to reduce background from beam particles passing through the stacks. The stacks were mounted at angles of 10, 16, 24, 35, 55, 80, 100, 125, 145, 156, 164, and 170 degrees. These angles were chosen in order to optimize the number of stacks that could be fitted into the chamber. Two detector stacks were placed at each angle: a thick stack to measure fragments with $5 \leq Z \leq 8$ and a thin stack to measure fragments with $7 \leq Z \leq 10$.

The target was mounted in the middle of the frame at 45° to the beam direction. The frames were segmented into three pieces for ease of transportation and were easily connected at run time. Figure 1 shows the detector configuration. In order to obtain a large dynamic range in cross section we conducted three exposures, each with different beam fluences, target thicknesses, and stack thicknesses. If we were to conduct only a single exposure, then we would not be able to obtain information at high cross section as the track densities in the plastic would be too high to analyze. With a lower beam fluence and a thinner target we can obtain high cross section measurements at low energy with good energy resolution. The beam energy at the entrance to the vacuum chamber was 105 MeV/nucleon. The energy at the center of the thickest target was ~101 MeV/nucleon.

The methods for processing the Lexan have been described elsewhere,[23,24] so only a brief description will be given here. The Lexan was exposed to ultraviolet light and etched in 6.25N NaOH to make tracks visible in a microscope. The tracks were etched long enough to form cylindrical holes that were detected by passing ammonia gas through the cylinders onto blueprint paper. The ultraviolet exposure enhanced the sensitivity of the plastic. Two exposures were used. The first was a three day exposure on each side of the sheets which allowed a cylinder to form in the last sheet before the end of the range for charge 5 and above. The second exposure was one day on each side per sheet and was used to detect charge 7 and above. This is useful because at a given range there is usually a much higher density of lighter charges. By going to a shorter UV exposure we can filter them out. The plastic is affected by UV in the 3000 A region. A meter sensi-

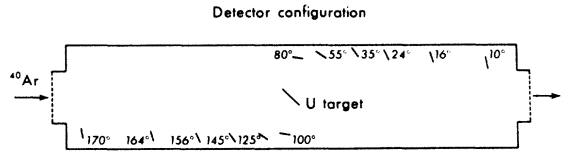

FIG. 1. The positions of the Lexan detectors and uranium target in the vacuum chamber.

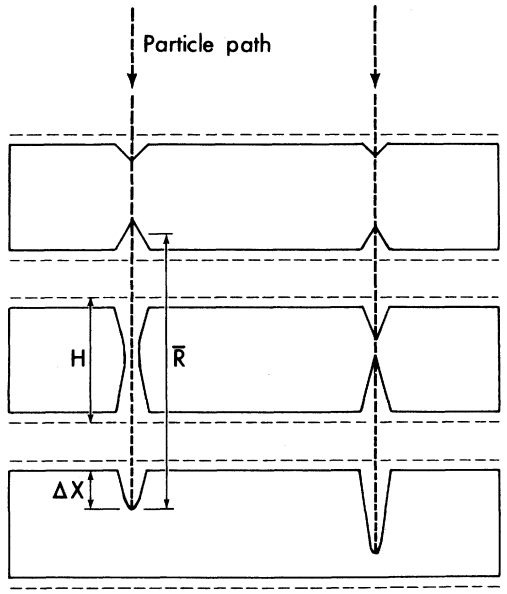

FIG. 2. Two etched particle tracks for the last three Lexan sheets at the end of range of the particle. The particle on the left would be detected in this experiment by the hole in the middle sheet. H is the sheet thickness before etching. ΔX is the track length in the last sheet after etching. $\bar{R}$ is the distance from the center of the cone to the point where the particle stopped. The particle on the right would not be detected.

tive to UV at 3600 A (mercury has a strong line there) was used to monitor the UV output. The UV bulbs tend to weaken appreciably after 1000 to 2000 h of use—about the total exposure time needed to process all of the sheets in the experiment. A large change in the UV output would effect charge assignments and detection efficiencies. We found the bulb output remained constant at the $\pm 10\%$ level, which is sufficiently stable to be negligible. The etch time for the sheets was 30 h. In the middle of the experiment it was necessary to change from etching in a small tank to a much larger tank. At this time the etch rate of the plastic changed slightly and the changing of the etch tanks is believed to be the culprit. We accounted for this by making charge assignments and detection efficiency assignments for each bulk etch rate V_g separately. The changes were not serious but it took an appreciable amount of time to correct for them.

Etched tracks can be divided into three classes—test tubes, cylinders, and cones—as shown in Fig. 2. When a particle stops in a sheet of plastic, the track can etch to the end of range and then etch at the bulk etch rate of the plastic, leaving a track that looks like a miniature test tube. Cylinders occur when the track etches through the whole sheet. If the track does not etch through the whole

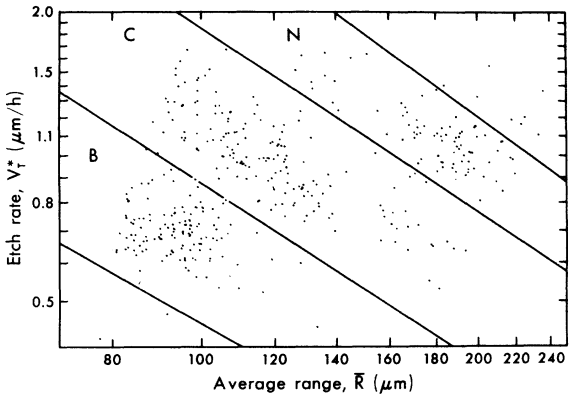

FIG. 3. Plot of the etch rate V_T^* vs average range $\bar{R}$ for 400 events from the 3 d UV on each side and 30-h etch.

sheet a cone pair will appear, one where the particle entered the sheet and another where it left. A measurement of the length of a cone allows us to compute the etch rate along the track. By measuring cone length, test tube length, and sheet thicknesses in between the cone sheet and test tube sheet, we can compute the distance from the cone to the end of range of the particle. With a knowledge of the track etch rate, V_T^* and the average distance to end of range, $\bar{R}$, we can determine the charge of the particle.

It is convenient to redefine the track etch rate as $V_T = V_T^* - V_g$ where V_g, the bulk etch rate of the plastic, is typically about 0.19 μm/h. Figure 3 shows a plot of V_T^* vs $\bar{R}$ for 400 points. We see that the points lie in distinct bands. From calibrations we know that $V_T \propto \bar{R}^{-1.6}$. We define the range-adjusted track etch rate $V_T(\text{at } 100\ \mu\text{m}) = V_T(\bar{R}) \times (\bar{R}/100)^{1.6}$ to be the measured track etch rate adjusted to 100 μm. We then make histograms [Figs. 4(a) and 4(b)] of the number of events vs V_T(at 100 μm). Distinct charge peaks are seen. The charge assignments are based on ^{12}C, ^{14}N, and ^{20}Ne cyclotron calibrations and on direct observation of ^{8}Li and ^{8}B tracks (via the reactions $^{8}Li \rightarrow {}^{8}Be \rightarrow 2\alpha$ and $^{8}B \rightarrow {}^{8}Be \rightarrow 2\alpha$, which lead to characteristic "hammer tracks").

As a further check on sheet thickness, and as a check on etch conditions, all sheets were weighed before and after etching. Sheet thickness fluctuations were taken into account when computing detection efficiencies. We found that preselecting the sheets greatly reduced the errors due to thickness fluctuations.

We measured approximately 5000 events. Until the measurement process can be fully automated it will be difficult to increase the number of events that can be measured in a single experiment. The total number of data points in the

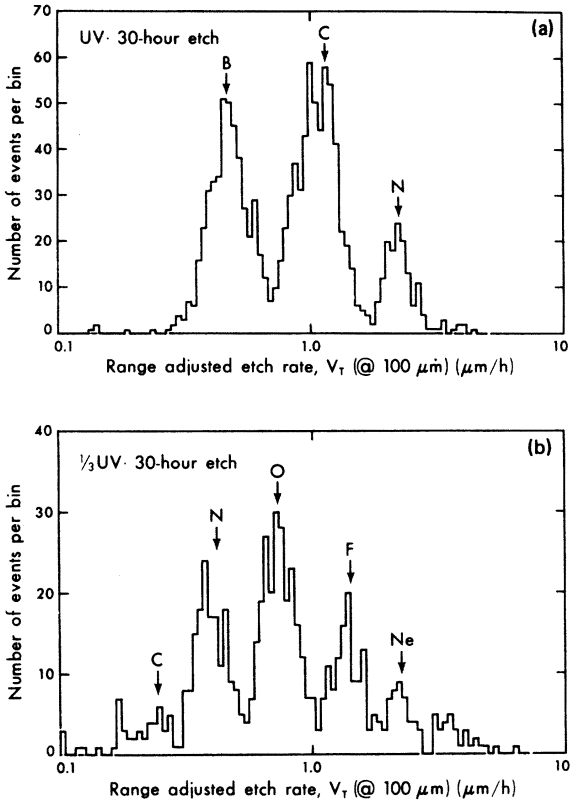

FIG. 4. Histograms for number of events vs range-adjusted etch rate V_T (at 100 μm). (a) Three day UV on each side and 30-h etch. (b) One day UV on each side and 30-h etch.

present work is not significantly greater than in Refs. 11 and 26 even though our measurements extend over a much wider dynamic range than in our previous experiments. Our data are more spread out than in previous experiments. This is done in order to obtain a good overall view of the cross section but at the expense of sacrificing small details in structure. An advantage of our detector is that if we then believe there may be structure somewhere it is usually possible to process more sheets later and to investigate the region in more detail.

EXPERIMENTAL RESULTS

We obtained double differential cross sections for the fragments boron, carbon, nitrogen, oxygen, fluorine, and neon. The data are plotted in Figs. 5–10. The lines drawn through the data are meant only as a guide to the eye.

The data show several interesting characteristics. The boron spectrum at 16 deg and at energies above 40 MeV/nucleon is nearly flat in contrast to the exponential falloff seen at larger angles. This effect may be due to projectile fragmentation. Low energies in the projectile frame are transformed to large values when seen in the laboratory. The exponential falloff in the data at large angles is characteristic of fragment distributions seen at higher beam energy. The dis-

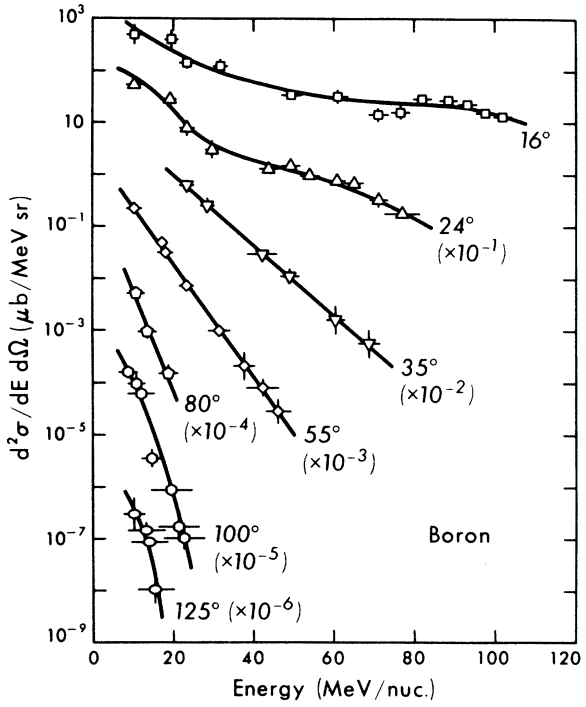

FIG. 5. Plot of boron data from 16° to 125°.

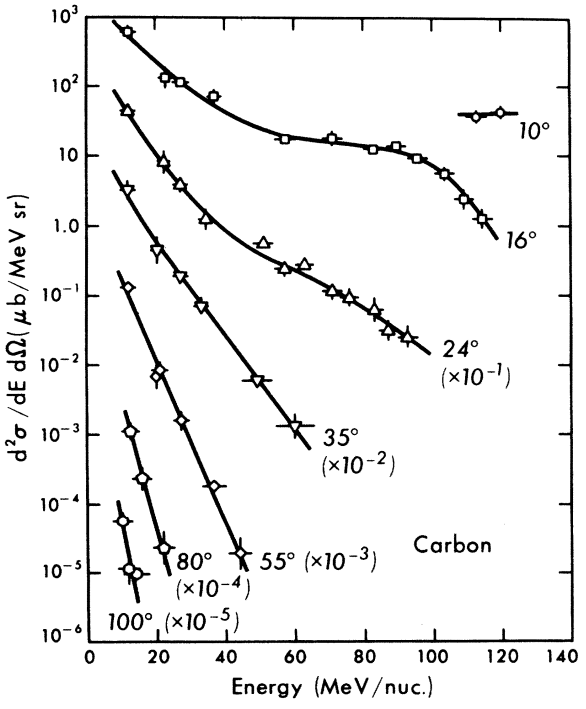

FIG. 6. Plot of carbon data from 10° to 100°.

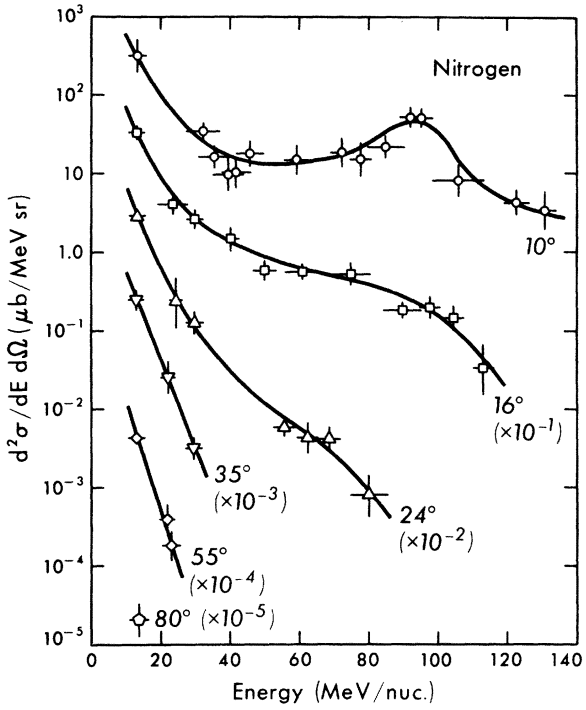

FIG. 7. Plot of nitrogen data.

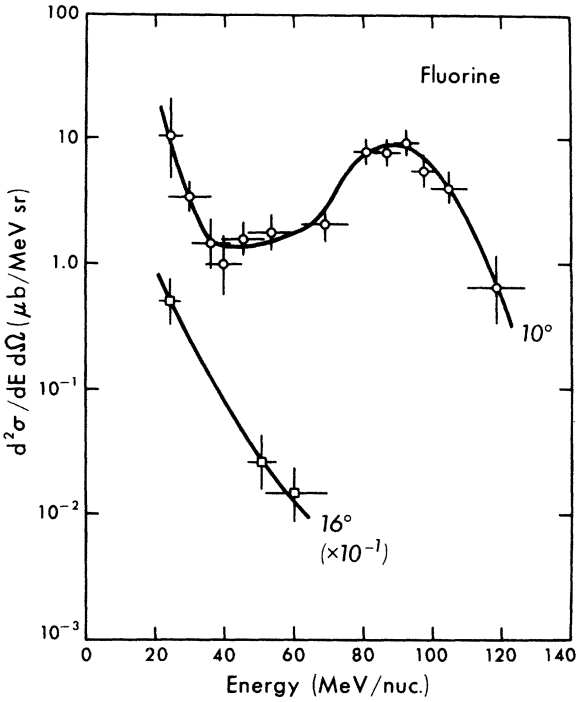

FIG. 9. Plot of fluorine data.

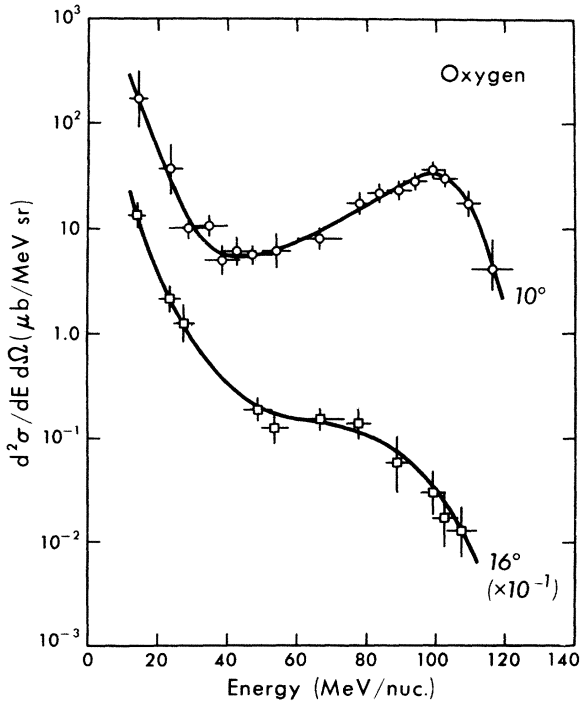

FIG. 8. Plot of oxygen data.

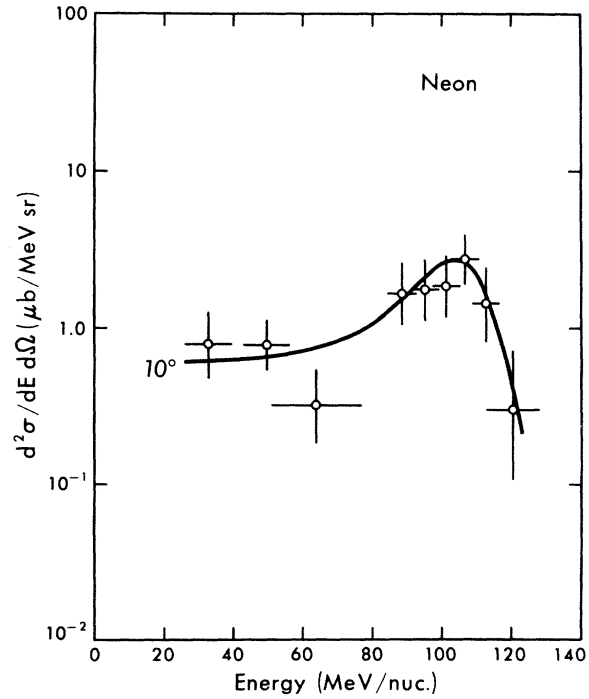

FIG. 10. Plot of neon data.

tributions at 10 deg clearly show projectile fragmentation peaks at the beam energy/nucleon. Beyond the beam energy/nucleon the cross sections drop rapidly. The distributions for carbon and boron appear to be quite similar in magnitude, but for higher mass the total cross section drops.

IV. DATA ANALYSIS

A. Thermal parametrization of the data

It is convenient to divide the data into two groups. The first group covers fragments which are presumably emitted in central collisions—low to intermediate energy nuclei emitted at all angles. The second group contains fragments that are apparently from the projectile and which are produced in peripheral collisions at small laboratory angles with nearly the beam velocity.

Let us assume that fragments are emitted thermally by a moving source. We shall take

$$\frac{d^2\sigma_i}{dEd\Omega} = \frac{\sigma_i}{2(\pi\tau)^{3/2}}\sqrt{E}\, e^{-E/\tau} \tag{11}$$

to be the nonrelativistic Maxwell-Boltzmann distribution in the moving frame for the fragments, where E is the kinetic energy and σ_i is the normalization for the production of the ith fragment. For central collisions, where we expect a large number of nucleons to be found in the source, we may take τ to be the temperature T. For peripheral collisions we take into account two-body kinematics by setting $\tau = \nu T$, with $\nu = A/(A-K)$. This preserves the relation between the Gaussian width σ and T [Eq. (6)], so our discussion of projectile fragmentation will be valid for either the thermal or sudden breakup models. We also expect that the normalization σ_i should be "reasonably" related to the partial production cross section for fragment i. As an obvious example, we note the normalization should not exceed the product of the total cross section for the reaction times the number of nucleons in the collision.

1. Fragments apparently from central collisions

Fits using a single source (3 parameters) gave poor results, so two sources (6 parameters) were used. For each source the three parameters were the temperature $\tau = T$, source velocity β, and normalization σ. Since the data cover a large dynamic range, the points that were included in each fit had to be carefully chosen. The procedure was to pick a set of points, determine the best fit using a chi-square minimization routine, and compare the fit to the data. Points that were located far from the fitted curves were rejected and a new fit was made. Usually points would be rejected because they were at small angles and contained contributions from projectile fragmentation. Most of the rejected points were then treated with the projectile fragmentation analysis.

A list of the parameters χ^2, the number of points fitted, and the angle and energy constraints are shown in Table I. The fits for boron, carbon, and nitrogen are shown in Figs. 11–13. The slower of the two sources has a velocity $\beta_s \sim 0.07$ and temperature $T_s \sim 27$ MeV. The faster source has a velocity $\beta_f \sim 0.17$ and temperature $T_f \sim 38$ MeV. Note that the values of χ^2, especially for boron, are fairly large. This is mainly due to the large dynamic range being covered. The boron data can be fitted better with the following restrictions: at 16° exclude energies >30 MeV/nucleon, at 24° exclude energies >40 MeV/nucleon, and at 35° exclude energies >60 MeV/nucleon. This fit gives a χ^2 of 106 for 33 points. The velocities and temperatures are $\beta_s = 0.0696$, $T_s = 23.2$, $\beta_f = 0.146$, and $T_f = 36.6$. If we exclude all 16° and 24° data from the fit the χ^2 is reduced to 50.9 for 26 points. The fitted velocities and temperatures are $\beta_s = 0.0778$, $T_s = 22.5$, $\beta_f = 0.155$, and $T_f = 35.1$. We see that the value of χ^2 has significantly improved while the source velocities and temperatures have changed only slightly. Similar improvements apply for carbon and nitrogen data.

We can compare the values of the parameters to those we would expect if either a target explosion or a nuclear fireball is the source of the fragments. For target explosion we assume that the uranium and argon nuclei recoil as a single entity. Energy and momentum conservation give the internal energy E_{int} and the recoil velocity β of the source. For the nuclear fireball only the participants, i.e., the nucleons in the classical overlap region, are involved in the reaction. The participants in the collision at optimal impact parameter, which occurs when the projectile is just totally enclosed by the target ($b = R_{\text{target}} - R_{\text{projectile}}$), give a velocity and temperature that are suitable averages for the fireball model. Using Eqs. (2)–(4) to calculate the target explosion temperature we obtain $\beta = 0.067$ and $T = 2.8$ MeV. For the fireball we obtain $\beta = 0.15$ and $T = 9.2$. If we treat these systems as partially degenerate Fermi gases rather than ideal gases we obtain $T = 8$ MeV for target explosion and $T = 17$ MeV for the fireball.[25]

We note that the slow source has a velocity corresponding to target explosion while the fast source has a velocity corresponding to the fireball. The source temperatures required to fit the data are much higher than those predicted by either Maxwell-Boltzmann or Fermi-Dirac statistics. We see that the problem of high temperatures seen at projectile energies of 400–500 MeV/nucleon[11] also

TABLE I. Fitted parameters using a thermal model for central collision data.

Element	σ_1 (μb)	β_1	τ_1 (MeV)	σ_2 (μb)	β_2	τ_2 (MeV)	Applicable energy regime (MeV/nucleon)
Boron	389 000	0.0696	23.2	75 200	0.146	36.6	16°: <30; 24°: <40; 35°: <30; 55° to 125°
Carbon	382 000	0.0746	28.2	33 300	0.170	39.4	16°: <30; 24°: <40; 35° to 100°
Nitrogen	287 000	0.0834	32.1	5980	0.215	42.8	10°: <45; 16°: <50; 24°: <65; 35° to 80°

appears at 100 MeV/nucleon. The anomalously high temperature is also seen at 100 MeV/nucleon for the fireball source. No corresponding comparison can be made with a fireball source at beam energies of 250 and 400 MeV/nucleon since the experimenters either did not report a temperature[14] for composite fragments, or did not consider it to be an adjustable parameter.[11]

There have been several suggestions to explain the discrepancies between the predicted and "measured" source temperatures. We expect that the production of composites will decrease the numbers of degrees of freedom of the source and decrease the effective nuclear mass [see Eq. (4)], thereby giving a higher temperature. For small increases in temperature this may be a reasonable explanation, but there are many cases where the temperature is a factor of 3 or more greater than expected. Since most of the emitted fragments are protons and a typical source has more than fifty nucleons, a sufficiently high temperature system to fit the data cannot be produced by the creation of a few composite particles.

Preequilibrium and nonthermal emission are also possible explanations of the high apparent temperatures. Stevenson has examined several mechanisms of nonthermal emission, including rotating and expanding sources.[24] He has found that these mechanisms do not give a satisfactory fit to the data for 500 MeV Ar + Au interactions. We note that the statistical model of Randrup and Koonin[17] may offer an explanation of the anomalous high temperature phenomena.

Since the excitation energies are small we should check to see how well the data are fitted by a Fermi-Dirac distribution as opposed to a Maxwell-Boltzmann distribution. Most of the observed fragments have kinetic energies exceeding the nu-

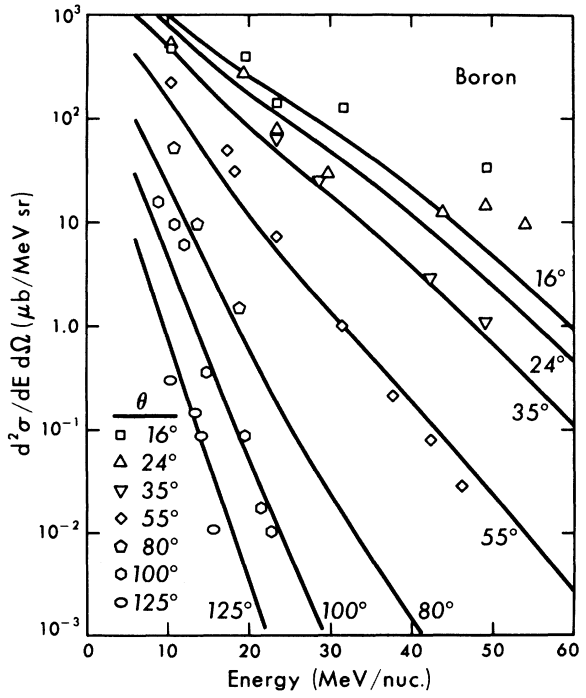

FIG. 11. Fit of two-source thermal model to the boron data.

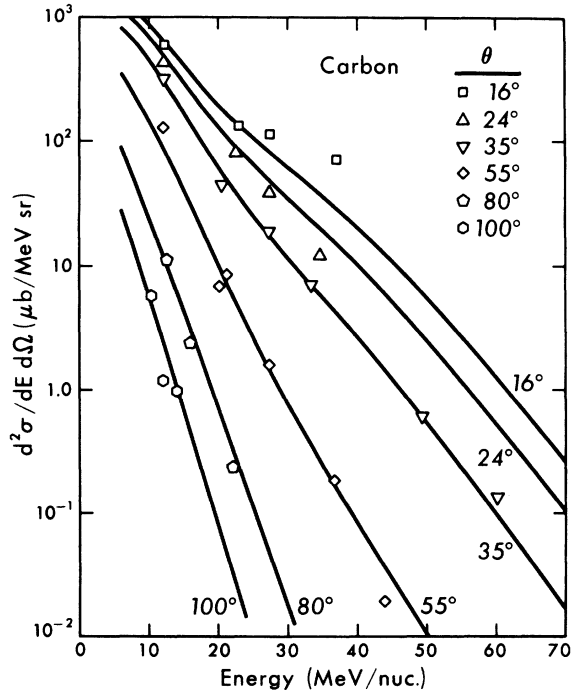

FIG. 12. Fit of two-source thermal model to the carbon data.

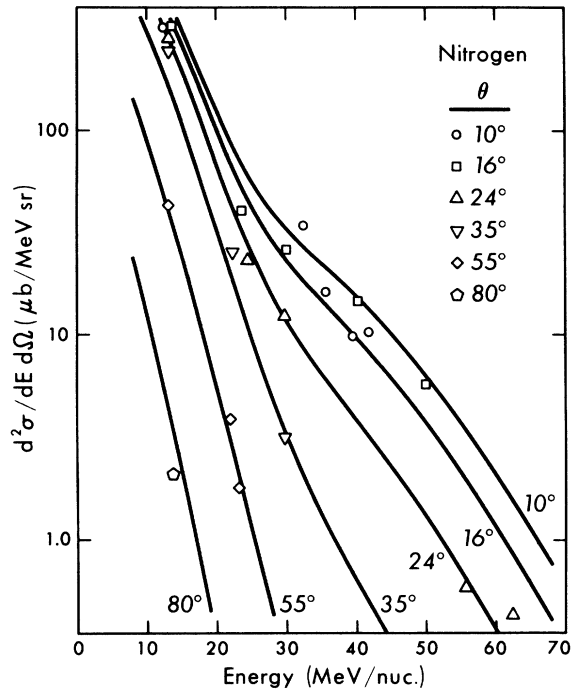

FIG. 13. Fit of two-source thermal model to the nitrogen data.

clear Fermi energy, so we would not expect much difference between a Maxwell-Boltzmann fit and a Fermi-Dirac fit. For carbon the Maxwellian fit gives a χ^2 of 30 for 25 points, with $\beta_s = 0.075$, $T_s = 28.1$, $\beta_f = 0.17$, and $T_f = 39.2$. The Fermi-Dirac fit is made using

$$\frac{d^2\sigma}{dEd\Omega} = \frac{\sigma_i}{2(\pi\tau)^{3/2}} \frac{1}{1+e^{(E-\mu)/\tau}}, \tag{12}$$

where μ is the chemical potential at temperature $\tau = T$. The fit gives $\chi^2 = 26$, $\beta_s = 0.079$, $T_s = 28.2$, $\beta_f = 0.17$, and $T_f = 39.2$. The χ^2 drops slightly but there is negligible change in the fitted parameters.

2. *Projectile fragmentation*

The projectile fragmentation peaks are broad and asymmetric. Since definite peaks are seen only at 10°, several different sets of parameters give fits of comparable quality. The data are insufficient to allow firm conclusions to be drawn.

Let us consider the oxygen data for energies greater than 40 MeV/nucleon. Viyogi *et al.*[26] measured a projectile fragmentation temperature of ≈8 MeV for 213 MeV/nucleon Ar + C for fragments emitted from zero to four degrees. They measured a partial cross section of ~81 mb for oxygen production. We can check to see if these results apply to our data. Figure 14(a) shows the predicted cross section for a source with $T = 8$ MeV, $\beta = 0.43$ (corresponding to a beam energy of 100 MeV/nucleon) using the values of the partial cross sections for oxygen isotopes reported by Viyogi *et al.* We see that the agreement is very poor. Different parameters are required to fit the data. If the partial cross sections are kept the same, but the temperature T is raised to 15 MeV [Fig. 14(b)], the peak is reproduced fairly well. Similar results apply for the fluorine and neon distributions. The data at 16° are obviously not described at all; they require a two-source model for a fit. The difference between our results and those of Viyogi *et al.* may be explained either by supposing that we are measuring the wings of some distributions beyond the smallest measured angle of 10°, or that the temperature (or equivalently the momentum width) may rise in the vicinity of 100 MeV/nucleon.

Before considering multiparameter fits we must check to see how sensitive the fits are to the effects of isotope distribution and target thickness. If the assumed isotope distribution varies from the true one, the fragment energy will be misassigned. The beam loses ~10 MeV/nucleon traveling through the thickest target and this will have an effect on the measured cross sections as shown in Fig. 15. In Fig. 15(a), an ^{16}O distribution with a correction for finite target thickness compared to an ^{16}O distribution with no target thickness correction. Viyogi *et al.*[26] have measured the cross sections for projectile fragments of ^{40}Ar on carbon at a beam energy of 213 MeV/nucleon. They have obtained isotope distributions for charges $8 \leq Z \leq 16$. The isotope distributions in our experiment are likely to be similar. We will use their measured distribution to see how sensitive our analysis is to isotope misassignment. In Fig. 15(b) an oxygen distribution with temperature $T = 15$ MeV assuming the isotope distribution of Viyogi *et al.*[26] is compared with a pure ^{16}O distribution. We see in both cases that the discrepancies are within the error bars of the data (Fig. 8). Using ^{16}O as the only oxygen present with no target thickness correction will not significantly alter the results. (Effects of isotopes and target thickness have also been observed for the "central collision" data and have also been found to be small.)

To fit the oxygen data well with thermal models at energies greater than 40 MeV/nucleon it is necessary to increase the number of parameters. One way to do this is to assume that there are two fast sources [Fig. 16(a)]. The fit gives $\chi^2 = 13$ for 20 points. The values of the fitted parameters are $\sigma_1 = 12500$ μb, $\beta_1 = 0.424$, $\tau_1 = 15$ MeV (corresponding to $T = 24$ MeV or a momentum width of 151 MeV/c) [Eqs. (6) and (8)] $\sigma^2 = 1200$ μb, $\beta_2 = 0.338$, and $\tau_2 = 34.8$ MeV. The first source has

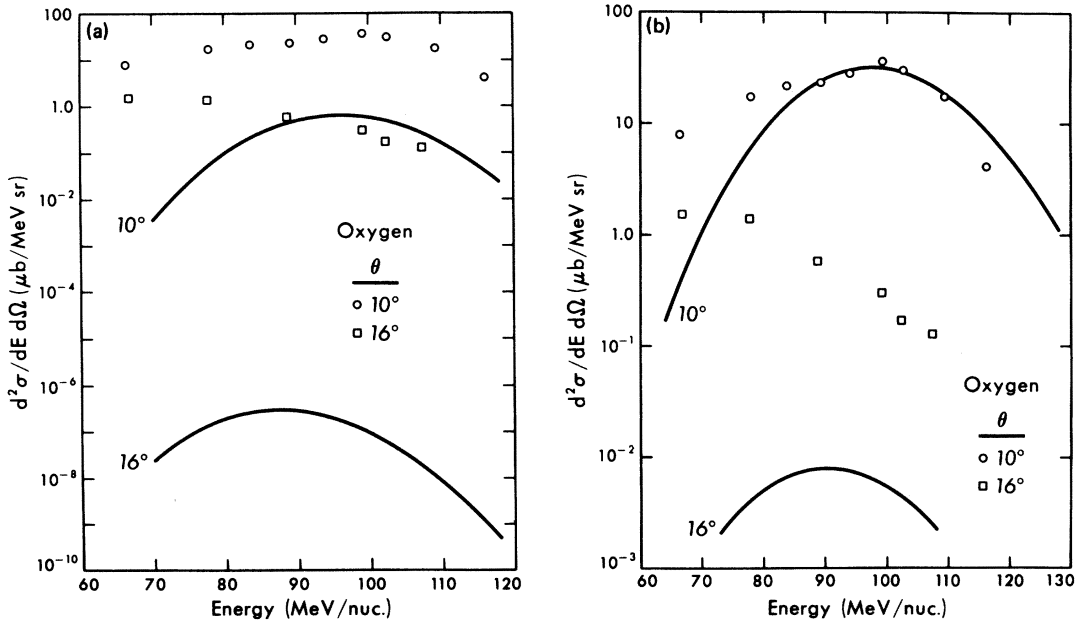

FIG. 14. Fits of a single source to oxygen projectile fragmentation. (a) Fit with a temperature of 8 MeV. (b) Fit with a temperature of 15 MeV.

a velocity close to that of the beam and a temperature much higher than that expected for conventional projectile fragmentation. We note that a beam velocity projectile fragment emitted at 10° in the laboratory is emitted at an angle ≈85° in the projectile frame. The effects of orbital dispersion as reported by Van Bibber *et al.*[20] may account for the apparent high temperature. The second source has a very high value of τ_2, but since we are unsure of its nature, we do not assign it a temperature. The second source implies that part of the projectile underwent a collision with the target nucleus with a resulting large transfer of momentum. This may not be the correct interpretation because the fact that the intermediate rapidity points can be fitted by a thermal source may be an accident.

The nitrogen data have also been fitted at 10°

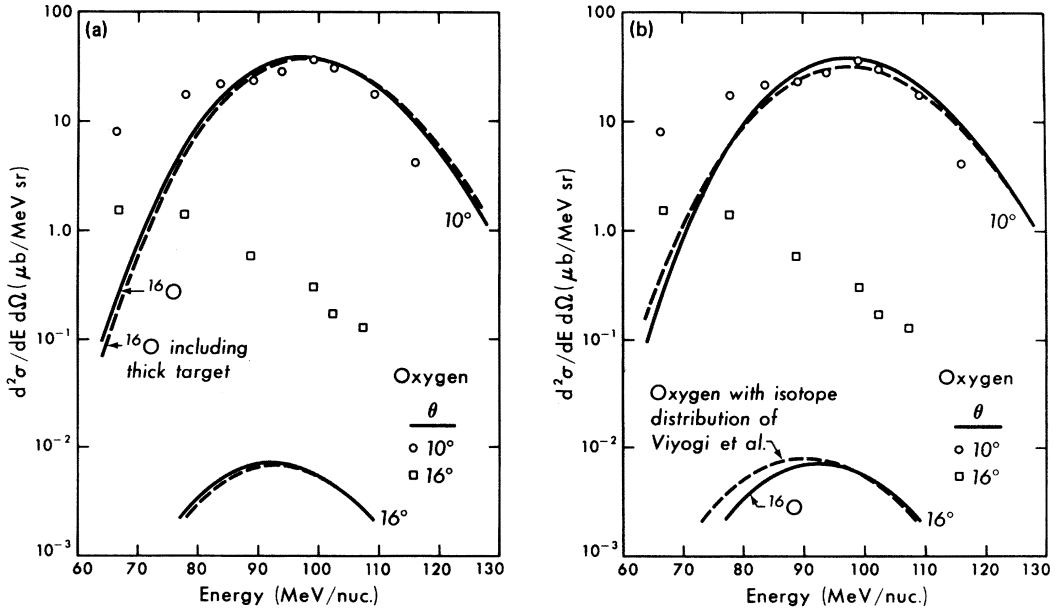

FIG. 15. (a) Effect of using a thick target on the distribution of oxygen from projectile fragmentation. (b) Effect of multiple isotopes on the distribution of oxygen from projectile fragmentation.

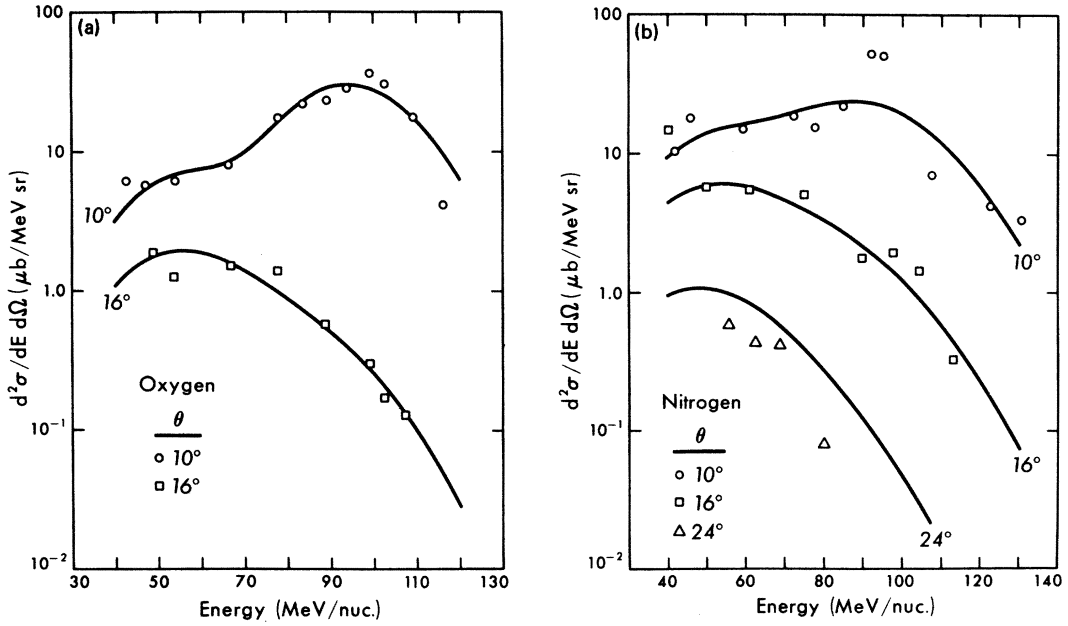

FIG. 16. Two-source thermal fits from projectile fragmentation. (a) Oxygen. (b) Nitrogen.

and 16° [Fig. 16(b)]. The results are $\chi^2=19.8$ μb for 17 points, $\sigma_1=4110$ μb, $\beta_1=0.416$, $\tau_1=20.6$ MeV, $\sigma_2=2760$ μb, $\beta_2=0.328$, $\tau_2=20.6$ MeV. Points with energies greater than 45 MeV/nucleon were included in the fit. The fit does not reproduce the peak at 10°, but the error bars in the data are fairly large. (See Fig. 7.) Note that at 24° the fit exceeds the data, increasing our suspicion that the large momentum transfer source may be fictitious.

The boron and carbon data that appeared to be due to projectile fragmentation were fitted at 16° and 24°. Two fast sources were necessary to obtain reasonable fits. For boron the best fit gives $\chi^2=10.8$ for 16 points, $\sigma_1=6.84\times10^8$, $\beta_1=0.424$, $\tau_1=5.4$ ($T=7.4$), $\sigma_2=13\,600$, $\beta_2=0.288$, $\tau_2=41.6$ [Fig. 17(a)]. The fit overshoots the data at 35°. The normalization cross section σ_1 for the beam velocity source is also much too high. By raising the temperature we can lower the normalization. A fit with the parameters $\sigma_1=543$, $\beta_1=0.424$, $\tau_1=11$ ($T=15.2$), $\sigma_2=13\,3300$, $\beta_2=0.284$, and $\tau_2=43.2$ gives a χ^2 of 15.2 [Fig. 17(b)]. The figure shows that the fit is still reasonably good although the problems at 35° have not been resolved. The carbon is fitted at 16° and 24° for energies above 50 MeV/nucleon. We obtain $\chi^2=11.3$ for 16 points, $\sigma_1=44\,300$ μb, $\beta_1=0.402$, $\tau_1=16.4$ ($T=23.4$), $\sigma_2=7060$ μb, $\beta_2=0.276$, and $\tau_2=45$ (Fig. 18). Note that the fit is close to the 10° points and is roughly in agreement with the data at 35°, which was fitted with the fireball source. A summary of the projectile fragmentation fits is given in Table II.

B. Invariant cross section and exponential in momentum

Contours of invariant cross section [$f=(1/p)(d^2\sigma/dEd\Omega)$] for boron are shown in Fig. 19. The coordinate axes are parallel and transverse momenta. The curves are obtained by drawing smooth curves through the data. The contours are roughly circular with centers around a parallel momentum $p_\parallel$ of about 1000 MeV/c. For large $p_\parallel$ the contours deviate from being circles due to effects of projectile fragmentation.

In the case of isotropic emission from a moving frame the contours form ellipses with $p_\parallel$ being one of the axes. For low source velocities $\beta_0 \ll 1$ these ellipses should be nearly circles. From locations of the centers of the circles we obtain the velocity of the source

$$\beta_0=\frac{p_\parallel}{M\gamma_0}\approx\frac{p'_\parallel}{M} \tag{13}$$

and from the radii of the circles we obtain the velocities β' of the fragments in the moving frame:

$$\beta'=\frac{p'}{M\gamma'}\approx\frac{p'}{M}. \tag{14}$$

We should note that these velocities refer to averages and are not representative of discrete sources.

Best fit circles were constructed for the invariant cross section contours using a χ^2 minimization routine. Both β_0 and β' were varied until the minimum χ^2 was found. Selected points, usually

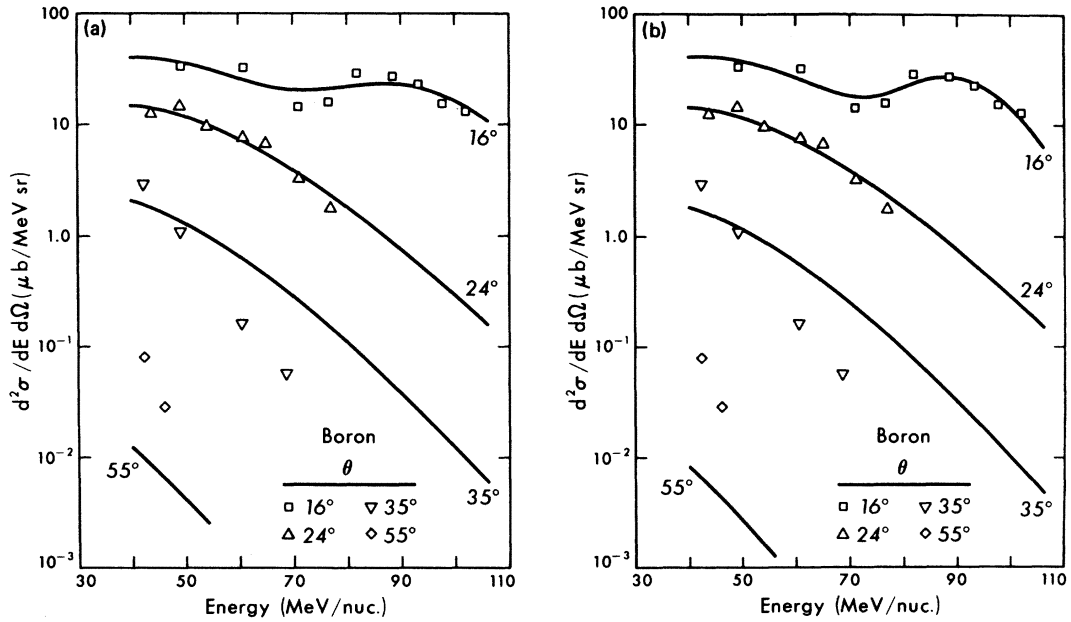

FIG. 17. Two-source thermal fits to high-energy boron data. (a) Fit with source parameters $\tau_1 = 5.4$, $\tau_2 = 41.6$. (b) Fit with source parameters $\tau_1 = 11$, $\tau_2 = 43.2$.

those at small angle and large $p_{\parallel}$, were excluded from the fits if they caused the contours to deviate seriously from being circular. A scatter plot of β_0 vs β' for the fragments boron through nitrogen is shown in Fig. 20. We note there is some correlation between β_0 and β'. The correlation appears poor here because there is still some contamination from projectile fragments at small angles. The graph looks much better if these contaminants are removed. The dependence of β' and β_0 has been studied for a number of experiments by Price and Stevenson.[27] They claim that the correlation of fragment velocity with source velocity independent of fragment mass shows that the source cannot be thermal in nature.

From the constructed circles we can determine the momentum p' of the fragments in the moving frame, and plot the values of p' as a function of invariant cross section (Fig. 21). The points shown in the figure are obtained from the boron, carbon, and nitrogen data. Contributions from projectile fragmentation are not included. Recall that the points are not data points but are obtained by drawing smooth curves through the data. Overlaid on the plot are curves for the reactions 400 MeV/nucleon Ne + U → ^{8}Li and boron.[13] The curve

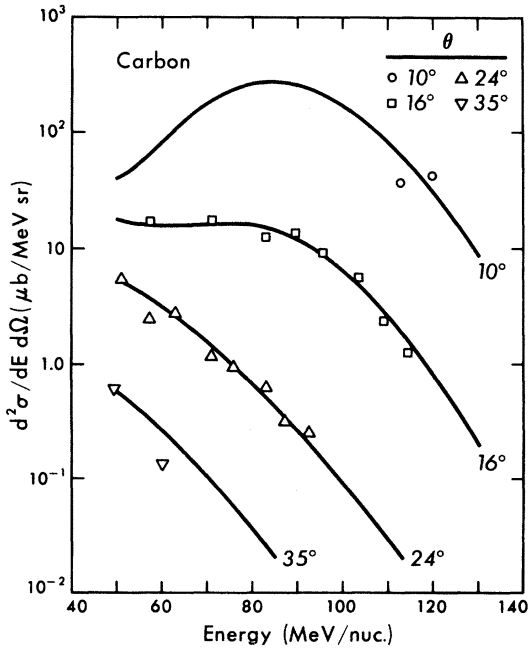

FIG. 18. Two-source thermal fit to high-energy carbon data.

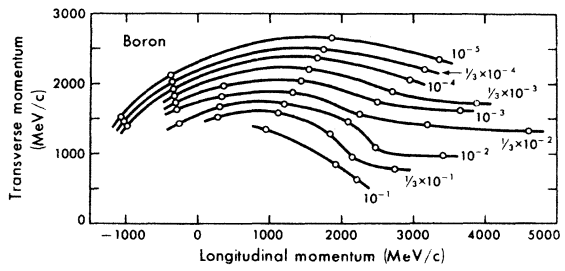

FIG. 19. Plot of contour of constant invariant cross section [μb/sr(MeV^2/c)] in transverse momentum $P_{\perp}$ vs longitudinal momentum $P_{\parallel}$ for boron fragments.

TABLE II. Fitted parameters using a thermal model for peripheral collision data.

Element	σ_1 (μb)	β_1	τ_1 (MeV)	T_1 (MeV)	σ_2 (μb)	β_2	τ_2 (MeV)	Applicable energy regime (MeV/nucleon)
Boron	6.84×10^8	0.424	5.4	9	13 600	0.288	41.6	16°: >40; 24°: >40
Carbon	44 300	0.402	16.4	23.4	7 060	0.276	45	16°: >50; 24°: >50
Nitrogen	4 110	0.416	20.6	31.7	2 760	0.328	41.8	10°: >45; 16°: >45
Oxygen	12 500	0.424	15	25	1 200	0.338	34.8	10°: >40; 16°: >40

for ^{8}Li is shown multiplied by three as an approximate correction for the other lithium isotopes. The plotted points follow the pattern of the universal curve of Price *et al.*[13] surprisingly well. The characteristic momentum associated with the plotted points is approximately $P_c = 190$ MeV/c. This compares to $P_c = 236$ MeV/c for 400 MeV/nucleon Ne + U and $P_c = 340$ MeV/c for 500 MeV/nucleon Ar + Au. Since all curves lie relatively close to one another this suggests that when comparing several curves, a change in slope (P_c) is compensated by a change in normalization (K) for some distribution $f = Ke^{-P/P_c}$. Alternatively, we might say that at some value of momentum in the moving frame, all invariant cross sections are basically identical, with the first order corrections being determined by P_c.

The origins of the universal curve still remain unknown. It is surprising that fragment data from reactions for projectile energies of 100 to 2100 MeV/nucleon all lie close to the same curve.

V. SUMMARY AND CONCLUSIONS

Data from the reaction 100 MeV/nucleon Ar + U → fragments have been presented. By conducting three exposures using different combinations of target thickness and beam fluence, we have been able to measure cross sections over a wide dynamic range. Fragments emitted from both central and peripheral collisions are observed.

The data have been fitted with thermal sources, each moving with a characteristic velocity and temperature. These sources are not discrete, but are believed to be in some sense an average over a continuum of sources. The data which are apparently due to central collisions can be interpreted in terms of emission of fragments from two sources, one corresponding to a system undergoing "target explosion" and the second from a nuclear fireball. The observed temperatures are higher than one would calculate using energy and momentum conservation for either Fermi-Dirac or Maxwell-Boltzmann statistics. The process

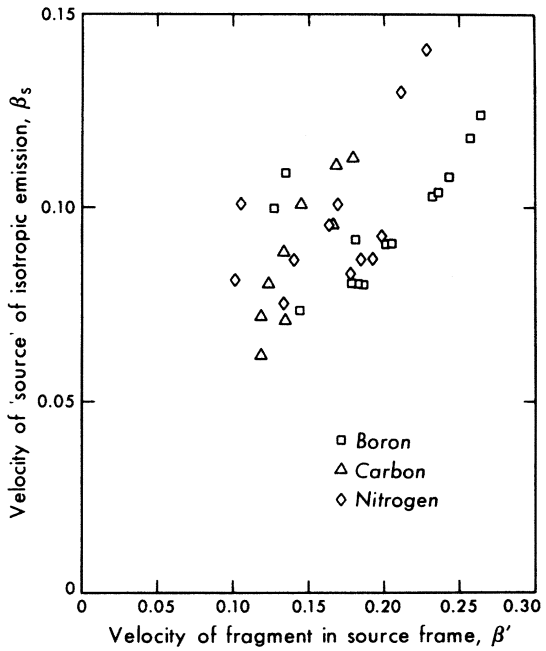

FIG. 20. Plot of source velocity β_0 vs fragment velocity in the moving frame β' for low energy B, C, and N.

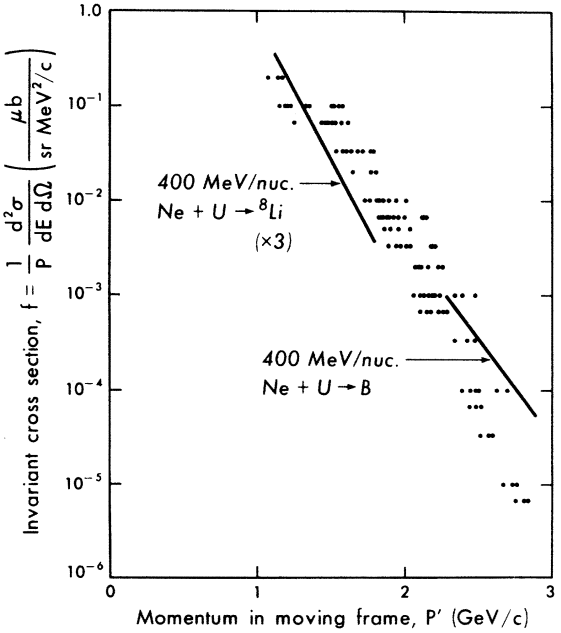

FIG. 21. Plot of invariant cross section vs momentum in the moving frame. Plotted points are from this experiment. The lines are from 400 MeV/nucleon Ne+U.

that produces these fragments appears to be of the same type that produces "slowly moving, highly excited nuclear matter" which is observed at beam energies of 400 and 500 MeV/nucleon, although its origin remains a mystery. The data lie along a previously discovered universal curve (or better termed "localized region") of invariant cross section vs momentum. The universal curve now encompasses fragments emitted in high energy heavy ion collisions for beam energies from 100 to 2100 MeV/nucleon.

The data which are apparently due to peripheral collisions have temperatures (or equivalently, widths) exceeding those seen in other projectile fragmentation studies. This may be due to orbital scattering of the projectile or to a peculiarity of looking at the tail of the projectile fragmentation distribution.

We see that the problems encountered in analyzing the data for experiments at 400 and 500 MeV/nucleon are already apparent at 100 MeV/nucleon. Correlation experiments could help determine if thermal equilibrium is reached before fragments are emitted in central collisions. Further theoretical developments are necessary before the interactions of relativistic heavy ions can be fully understood.

We thank Colleen Dunlavy for assistance with the microscope measurements and P. B. Price for helpful conversations.

[1]For a recent review, see A. S. Goldhaber and H. H. Heckman, Annu. Rev. Nucl. Sci. 28, 161 (1978).
[2]A. Poskanzer, Nature (London) 278, 17 (1979).
[3]J. Stevenson, Phys. Rev. Lett. 41, 1702 (1978).
[4]Y. Yariv and Z. Fraenkel, Phys. Rev. C 20, 2227 (1979).
[5]R. K. Smith and M. Danos, in Proceedings of the Topical Conference on Heavy-Ion Collisions, Fall Creek Falls, Tennessee, 1977, Report No. CONF 77-602, p. 363.
[6]J. Gosset, J. I. Kapusta, and G. D. Westfall, Phys. Rev. C 18, 844 (1978).
[7]A. A. Amsden, A. S. Goldhaber, F. H. Harlow, and J. R. Nix, Phys. Rev. C 17, 2080 (1978).
[8]A. S. Goldhaber, Phys. Lett. 53B, 306 (1974).
[9]A. Mekjian, Phys. Rev. Lett. 38, 640 (1977).
[10]H. H. Gutbrod, A. Sandoval, P. J. Johansen, A. M. Poskanzer, J. Gosset, W. G. Meyer, G. D. Westfall, and R. Stock, Phys. Rev. Lett. 37, 667 (1976).
[11]J. Stevenson, P. B. Price, and K. Frankel, Phys. Rev. Lett. 38, 1125 (1977).
[12]P. Siemens and J. O. Rasmussen, Phys. Rev. Lett. 42, 880 (1979).
[13]P. B. Price, J. Stevenson, and K. Frankel, Phys. Rev. Lett. 39, 177 (1977).
[14]G. D. Westfall, J. Gosset, P. J. Johansen, A. M. Poskanzer, W. G. Meyer, H. H. Gutbrod, A. Sandoval, and R. Stock, Phys. Rev. Lett. 37, 1202 (1976).
[15]J. Gosset, H. H. Gutbrod, W. G. Meyer, A. M. Poskanzer, A. Sandoval, R. Stock, and G. D. Westfall, Phys. Rev. C 16, 629 (1977).
[16]M. Ta Cheung and E. Moeller, Phys. Rev. Lett. 41, 1352 (1978).
[17]J. Randrup and S. Koonin, LBL Report No. 10959 (to be published).
[18]J. Randrup, private communication.
[19]D. E. Greiner, P. J. Lindstrom, H. H. Heckman, B. Cork, and F. S. Bieser, Phys. Rev. Lett. 35, 152 (1975).
[20]K. Van Bibber, D. L. Hendrie, D. K. Scott, H. H. Weiman, L. S. Schroeder, J. V. Geaga, S. A. Chessin, R. Truehaft, Y. J. Grossiord, and J. O. Rasmussen, Phys. Rev. Lett. 43, 840 (1979).
[21]G. D. Westfall, R. G. Sextro, A. M. Poskanzer, A. M. Zebelman, G. W. Butler, and E. K. Hyde, Phys. Rev. C 17, 1368 (1978).
[22]S. Nagamiya, L. Anderson, W. Brückner, O. Chamberlain, M-C. Lemaire, S. Schnetzer, G. Shapiro, H. Steiner, and I. Tanihata, Phys. Lett. 81B, 147 (1979).
[23]R. L. Fleischer, P. B. Price, and R. M. Walker, *Nuclear Tracks in Solids: Principles and Applications* (University of California Press, Berkeley, 1975).
[24]J. Stevenson, Ph.D. thesis, University of California, Berkeley, 1977 [Report No. LBL-7192, 1977 (unpublished)].
[25]E. C. Stoner, Philos. Mag. 28, 257 (1939).
[26]Y. P. Viyogi, T. J. M. Symons, P. Doll, D. E. Greiner, H. H. Heckman, D. L. Hendrie, P. J. Lindstrom, J. Mahoney, D. K. Scott, K. Van Bibber, G. D. Westfall, H. Wieman, H. J. Crawford, C. MacParland, and C. K. Gelbke, Phys. Rev. Lett. 42, 33 (1979).
[27]P. B. Price and J. Stevenson, Phys. Lett. 28B, 197 (1978).